Screening waves from steps and defects on Cu(111) and Au(111) imaged with STM: Contribution from bulk electrons

L. Petersen, P. Laitenberger, E. Lægsgaard, and F. Besenbacher
Institute of Physics and Astronomy and Center for Atomic-scale Materials Physics, University of Aarhus, DK-8000 Aarhus C, Denmark
(Received 23 March 1998)

By studying two-dimensional (2D) Fourier transforms of scanning tunneling microscopy (FT-STM) images, we obtain information about the role of surface states versus bulk states in the screening of defects and step edges at the close-packed Cu and Au surfaces. The STM images, obtained at low temperature and low bias voltage, exhibit wave interference patterns originating from the energy-resolved Friedel oscillations of surface-state electrons created by the screening of surface defects. The FT-STM pictures directly yield images of the 2D surface Fermi contour. Here we present results for Cu(111) and Au(111) surfaces, which reveal the existence of an additional contour in the FT-STM power spectrum. This contour is related to the ''neck'' of the bulk Fermi surface as accounted for by a simple model. The results give information about the role that both bulk and surface-state electrons play in the screening of defects at or near the surface. We find that the surface-state electrons dominate the screening of step edges on Au(111). [S0163-1829(98)07235-X]

I. INTRODUCTION

The concept of screening, i.e., the rearrangement of charge density to minimize the effect of an external perturbing potential, plays an important role in many aspects of solid-state physics. In linear response theory, the response of the electron gas of a metal to a disturbing potential is governed by the response function $\chi(\mathbf{q},\omega)$. The equation for computing this function was first derived by Lindhard[1] and relates the screening to the Fermi surface of a metal, defined by the equation $\varepsilon(\mathbf{k})=E_F$. The dimensionality of the electron gas as well as the detailed geometric shape of the Fermi surface play a crucial role in determining the nature of the response function and consequently the nature of screening. In general, the lower the dimensionality, the more pronounced are the screening effects.

At the surface, special electronic states exist as a consequence of the reduced translational symmetry. Such a state is confined in a narrow region perpendicular to the surface, thus constituting a (quasi) two-dimensional (2D) electron gas, and is termed a surface state. By definition this state only exists in bulk band gaps. If it crosses the Fermi level, it gives rise to a 2D Fermi contour, in complete analogy with the bulk Fermi surface. The surface-state electrons will participate in the screening at the surface. Due to the nature of the Lindhard response function,[1] the response of the free electron gas to a localized external potential is to create oscillations in the charge density around the disturbance. These have a wavelength $\lambda=2\pi/2k_F$, where k_F is the magnitude of the wave vector of the electrons at the Fermi energy E_F. Consequently, there is a direct relation between the Fermi contour and the screening wave pattern at the surface. If the contour is anisotropic, so is the screening wave pattern. The shape of the contour also influences e.g. the surface phonon spectrum (Kohn anomalies) and the electronic transport properties of the surface.[2] The surface Fermi contour may also reflect possible instabilities in the 2D electron gas (Fermi surface nesting).[3]

Since the Fermi surface dictates the response of the electrons to a static or dynamic disturbance via the response function as well as the electrical, magnetic, and structural properties of a metal,[2,4] it is important to determine its detailed shape. In the simple Sommerfeld model of a metal in which the electrons are treated as a gas of free particles, the bulk Fermi surface is a simple sphere. For real metals, the periodic one-electron potential provided by the nuclei and the other electrons, causes the Fermi surface to be more complicated. The Fermi surfaces for Cu and Au, for instance, are spheres with ''necks'' pointing out towards the $\langle 111\rangle$ directions. The bulk Fermi surfaces of many metals have in the past been mapped out experimentally utilizing the de Haas-van Alphen and the magnetoacoustic effects.[2] The time-honored technique for experimentally determining the surface Fermi contour is angle-resolved photoemission spectroscopy (ARPES).[4] For the Cu(111) and Au(111) surfaces, it has been found that free electron-like surface states with parabolic dispersion exist in the projected bulk band gap in the before mentioned ''necks.''[5]

Recently, a new approach to determine surface Fermi contours has been presented, namely the *Fourier transform-scanning tunneling microscopy* (FT-STM).[6–8] This simple technique is based on the ability of the STM to image the above mentioned oscillations in the electron density at the surface caused by electronic screening of point defects and step edges. The power spectrum of a 2D Fourier transform of such STM images (a FT-STM image) has been shown to image the 2D Fermi contour of the surface state directly, as demonstrated for example in the case of Be(0001) (Ref. 6) and Be(1010).[7] The energy resolution of the STM is superior compared to the one obtainable at present synchrotron radiation facilities using the ARPES technique, and the momentum resolution is similar.[8]

Here we report on STM measurements showing wave interference patterns due to screening of defects and steps on the Cu(111) and Au(111) surfaces. In the resulting FT-STM images, we observe not only the 2D circular Fermi contour resulting from the contribution of surface-state electrons to

 © 1998 The American Physical Society

the screening waves, but simultaneously we see a contribution from the edge of the *bulk* 3D Fermi surface ''neck'' in the FT-STM power spectrum image. Previously the STM studies by Crommie *et al.*[9] and Avouris *et al.*[10] have revealed the screening oscillations in the local density of states on the close-packed Cu and Au surfaces, but they did not report on any waves with wavelengths corresponding to the bulk Fermi surface. Screening waves due to bulk electrons have been observed from subsurface noble gas bubbles in aluminum, but these oscillations were mainly traveling towards the surface,[11] as opposed to the screening oscillations presented here, which are traveling along the surface. The fact that we observe both waves from surface-state electrons as well as waves due to bulk electrons implies that we should be able to study interesting questions such as the importance of surface states versus bulk states in screening at the surface, i.e., if bulk electrons contribute differently to screening of stepedges and impurities at the surface and whether a coherent coupling of surface states and bulk states exists.

II. EXPERIMENTAL DETAILS

The STM images of the Cu(111) and Au(111) surfaces discussed in this paper were all obtained at very low bias voltages (≈ 1 mV range) and low temperatures (140–160 K). The microscope used is a home-built, high-stability variable temperature STM, capable of operating between 120 and 350 K.[12] It is installed in an ultra high vacuum chamber with a base pressure below 1×10^{-10} torr, which is equipped with standard techniques for surface cleaning and characterization. The crystals are cleaned by sputtering with 1–2 kV Ne ions followed by annealing to 790 K (Au) and 830 K (Cu), respectively. This treatment results in well-ordered terraces with a width of ≈ 1000 Å. A small number [i.e., well below the detection limit ($\approx 1-2\%$) of Auger electron spectroscopy] of point defects/impurities are present in the terraces. Together with the step edges, these act as sources for the electronic screening waves.

III. THEORY

The wave patterns observed in the STM images are standing waves in the local density of states (LDOS) created by the screening of point defects and step edges. The electrons in the surface states on Cu(111) and Au(111) can be considered to constitute a free-electron-like 2D electron gas, and following the Friedel approach to screening,[13] the electron wave functions have the form of standing waves extending out from the scatterers. To calculate the resulting charge density $\rho(\mathbf{r})$, one has to sum over all occupied states, i.e.,

$$\rho(\mathbf{r}) = e \sum_{\mathbf{k}\ \mathrm{occ.}} |\psi_{\mathbf{k}}(\mathbf{r})|^2, \tag{1}$$

where $\psi_{\mathbf{k}}(\mathbf{r})$ is calculated in the presence of the scatterer. In the case of a free-electron gas, this leads to oscillations in the charge density with a wave vector $q=2k_F$, the so-called Friedel oscillations.[13] The factor of two is explained by the fact that it is the square of the wave function we are probing. The amplitude of these oscillations falls off with the distance from the scatterer as $1/r^a$, where $a>0$ depends on the dimensionality of the electron gas and the scatterer. In general, the amplitude falls off faster in 3D than in 2D. For the case of screening of an infinite potential barrier (a step edge) with a 2D free-electron gas, for instance, the result is $\rho(x) \propto \pi k_F^2/2[1-J_1(2k_Fx)/k_Fx]$.[10] Here x is the distance from the step, and J_1 is a Bessel function, which for large arguments behaves as $J_n(x)\sim\sqrt{2/\pi x}\cos(x-[2n+1]\pi/4)$, leading to $a=\frac{3}{2}$ in this particular case.

However, the STM does not image the entire charge density $\rho(\mathbf{r})$. According to the simple model of Tersoff and Hamann,[14] a constant current STM image obtained at low bias voltage can be interpreted as an image of the LDOS at the Fermi level E_F measured at the apex of the tip ($\mathbf{r}_0$), that is, the STM picks out the contribution to the charge density coming from electrons with energy close to the Fermi energy. Thus we have,

$$I_t \propto \sum_{\mathbf{k}\ \mathrm{occ.}} |\psi_{\mathbf{k}}(\mathbf{r}_0)|^2 \delta[\varepsilon_F - \varepsilon(\mathbf{k})] \equiv \mathrm{LDOS}(E_F, \mathbf{r}_0). \tag{2}$$

This contribution, which can be regarded as an energy-resolved Friedel oscillation, is also oscillatory with a wave vector $q=2k_F$, but the amplitude only falls off as $1/r^{a-1}$. This facilitates the experimental observations because the waves extend farther out from the scatterer, and can be seen as a consequence of the relationship between peak widths in direct and reciprocal space: A narrow distribution in reciprocal space leads to a broad distribution in direct space.

The effects of finite temperature can also be understood using the relationship between distribution widths in direct and reciprocal space. At finite temperatures, the Fermi-Dirac distribution broadens slightly around the Fermi level, leading to what may be thought of as a slightly broadened Fermi contour. The consequence of this broadening in reciprocal space is a narrowing in direct space, i.e., the amplitude fall off of the waves increases with temperature (see also Avouris *et al.*).[10] Thus, in order to get oscillations extending far away from the scatterer and thus sharp contours in the Fourier transform (FT), low temperatures are needed. But the oscillations may be visible even at room temperature.[15]

IV. EXPERIMENTAL RESULTS AND DISCUSSION

Whereas the clean Cu(111) surface is unreconstructed, Au belongs to the class of $5d$ metals of which the clean surfaces are reconstructed, and Au(111) exhibits the characteristic $(23\times\sqrt{3})$ herringbone reconstruction. In addition to a hexagonal arrangement of the individual Au atoms in the surface layer, the STM images of the Au(111) surface depict two bright stripes running along the $\langle 112\rangle$ direction within the reconstructed unit cell.[16] Along the perpendicular $\langle 110\rangle$ direction, 24 surface Au atoms are observed per unit cell on 23 bulk lattice sites, which implies that the reconstruction originates from a contraction of 4.4% of the top-layer Au atoms in this direction. This contraction induces a surface elastic strain, which results in a stacking fault domain structure involving periodic transitions between Au surface regions with fcc stacking and hexagonal close-packed (hcp) stacking. The gradual transition between fcc and hcp stacking domains creates the 0.2 Å corrugation lines running along the $\langle 112\rangle$ direction. The wider transition regions are identified as the fcc regions and hence fcc surface stacking is energetically more

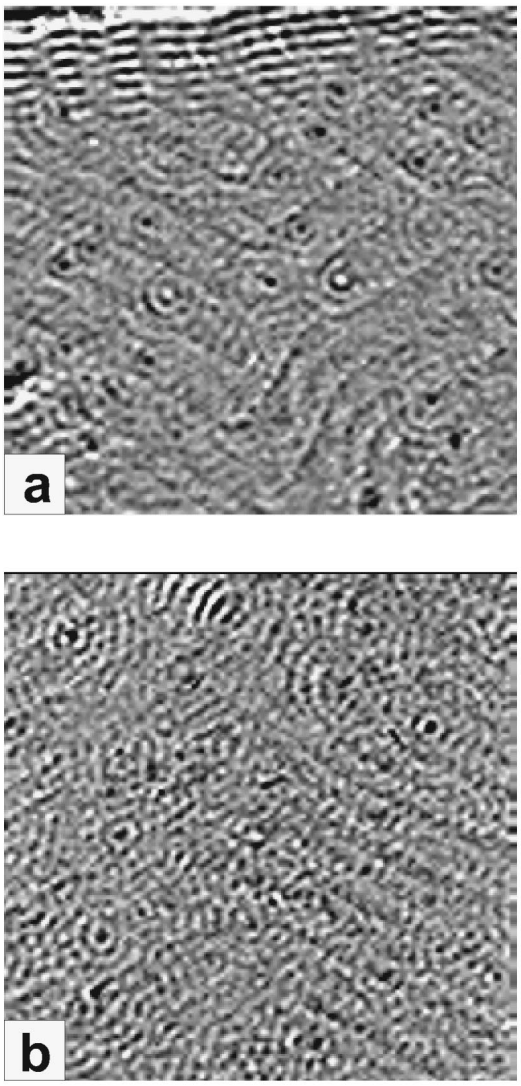

FIG. 1. (a) STM image of Au(111) ($V_t = 1.2$ mV, $I_t = 1.5$ nA, 610×610 Å^2) acquired at low temperature (150 K). A standing wave pattern extending out from defects and a step edge in the top of the image are clearly visible. The reconstruction lines are vaguely visible as well. (b) STM image of Au(111) ($V_t = -1.5$ mV, $I_t = -3.2$ nA, 610×610 Å^2) acquired at low temperature (140 K). Notice how the wave pattern seems to be slightly more ''blurred'' than is the case in (a). The images have been slightly processed to enhance the oscillations.

favorable than hcp stacking, as is the case in the bulk.

Figure 1(a) depicts a 610×610 Å^2 constant current STM image, obtained at a bias voltage of 1.2 mV (measured positive with respect to the sample, i.e., electrons tunnel from filled tip states into empty surface states) and at a temperature of 140 K. The herringbone reconstruction lines are observed to be vaguely visible under a complex interference pattern of waves extending out from point defects and the step edge in the upper left corner. The corrugation of the wave pattern is approximately 0.1 Å (rms), whereas the corrugation of an atomically resolved image is typically of the order 0.12 Å (rms). It should be noted that the waves are no longer imaged in constant current mode at these temperatures if the bias voltage is increased even slightly ($\geqslant 10$ mV). Part of the reason for this is that an increased

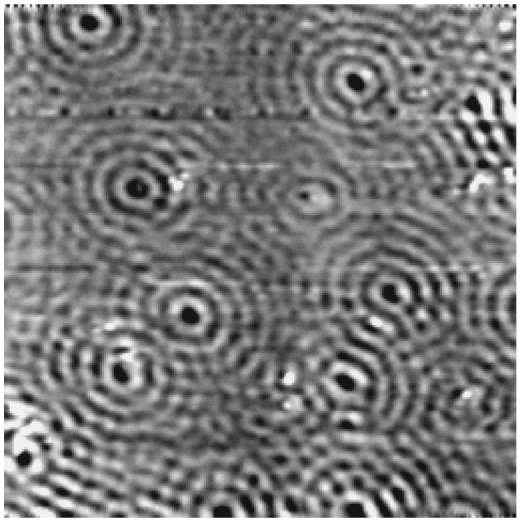

FIG. 2. STM image of Cu(111) ($V_t = -2.4$ mV, $I_t = -1.7$ nA, 420×420 Å^2) acquired at low temperature (150 K). Defects create a standing electron wave pattern.

voltage causes the tip to retract, washing out the wave structure because the corrugation depends on the tip-sample distance.

Sometimes a different tip condition exists and the wave interference images appear slightly ''blurred,'' as seen for example in the STM image shown in Fig. 1(b). As was the case with the image in Fig. 1(a), it is obtained at low bias voltage (-1.5 mV) and low temperature (140 K). Below, we shall discuss the differences between Figs. 1(a) and 1(b), but at this point it should be noted that the differences cannot be correlated with differences in the tunneling parameters (bias polarity) or the sample temperature.

Figure 2 shows a 420×420 Å^2 STM image (constant current) of Cu(111), obtained again at low bias voltage (-2.4 mV) and at low temperature ($T \sim 150$ K). An interference wave pattern similar to that observed for Au is seen, with circular screening waves originating from point defects/impurities and step edges. In the case of Cu(111), the corrugation of the wave pattern is of the order 0.09 Å (rms), whereas the atomic corrugation of the clean Cu(111) surface is of the order 0.13 Å (rms). In order to extract information about the wavelength of the energy-resolved Friedel oscillations, we use the FT-STM technique, i.e., we Fourier transform the STM images. The resulting power spectra are shown in Figs. 3(a)–(b) and 4 for Au(111) and Cu(111), respectively; light colors imply large Fourier components. In the following we will discuss the interpretation of the FT-STM images.

In Fig. 3(a) (Au) a ring is seen in the FT, which indicates that the wave pattern in the STM image consists of single wavelength plane waves running isotropically in all directions. As mentioned in the theory section above, the electrons that contribute to the low-bias STM images are the ones with an energy close to the Fermi level. The only allowed wave vectors at this energy are those lying on the Fermi contour and consequently these are the only ones contributing to the observed wave pattern. Since a Fourier transform reveals the wave vectors creating the direct space image, the FT in Fig. 3(a) *directly gives a map of the Fermi*

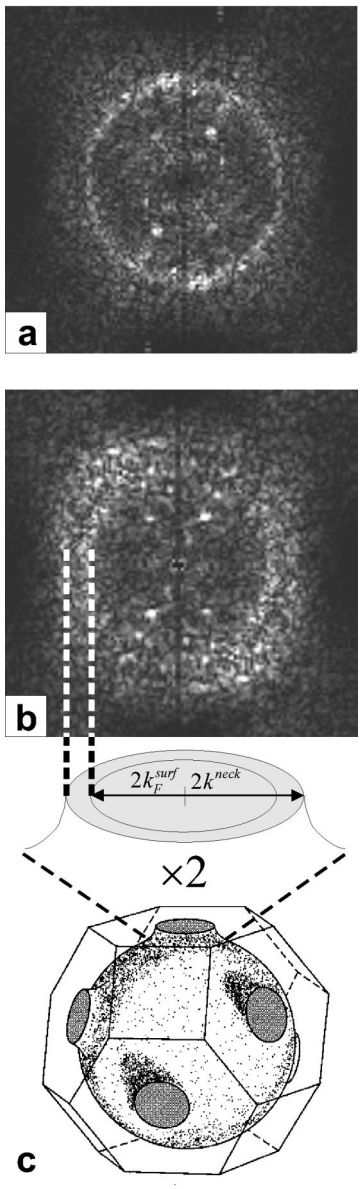

FIG. 3. (a) Power spectrum of the Fourier transform of Fig. 1(a). Light colors correspond to large Fourier components. The circle is a direct image of the surface-state Fermi contour (scaled with a factor of two). The dark-vertical line in the middle is due to noise reduction employed in the original image. (b) Power spectrum of the Fourier transform of Fig. 1(b). Two concentric circles are visible. (c) Illustration of the origin of the two concentric circles seen in Fig. 2(b).

contour of the surface state on Au(111), scaled with a factor of two.[6] The vertical lines in the center of the images are due to line noise in the original STM images, which generate noise Fourier components. In the case of Au(111) [Figs. 3(a) and (b)], one should also note the spots lying on a line through the origin. These are due to the periodicity of the reconstruction and can be used for internal calibration of the Fourier transform. By measuring the radius of the ring in Fig. 3(a), we can determine k_F for the surface state on Au(111) and find $k_F = 0.166 \pm 0.020$ Å^{-1}. The uncertainty is estimated on the basis of the calibration of the STM.

When comparing Fig. 3(b) with Fig. 3(a), we see an interesting and important difference: There are *two* concentric

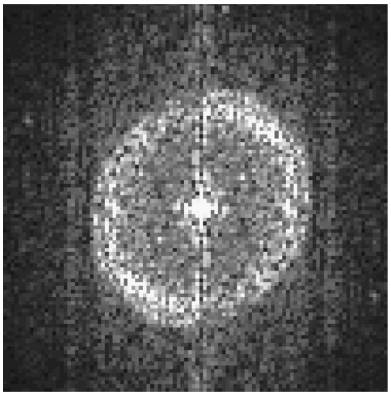

FIG. 4. Power spectrum of the Fourier transform of Fig. 2. The enhanced intensity in the north-east and south-west directions is due to the presence of a step just outside the lower left corner of the image in Fig. 2. The circle is slightly elliptical because of a distortion of the STM image caused by thermal drift.

rings in the FT. They appear broader or ''blurred'' compared to the ring in Fig. 3(a) and indicate that the wave pattern in Fig. 1(b) is a superposition of waves with two slightly different wavelengths. It should be noted that the extra ring is not an experimental artifact. A double tip would only give rise to a phaseshift in the Fourier transform and would thus not be observed in the power spectrum. Likewise, a modulation due to e.g. the reconstruction would not result in concentric rings, but rings with shifted centers. The inner ring is recognized as the Fermi contour of the surface state. As will become clear below, the outer ring is due to a contribution to the screening waves from electrons coming from the ''neck'' of the bulk Fermi surface. From the radius of the outer ring, we determine $k_{F,\mathrm{outer}} = 0.21 \pm 0.01$ Å^{-1}, which is in very good agreement with measurements of the bulk neck radius utilizing de Haas-van Alphen and magnetoacoustic effects, yielding the exact same result $k_{F,\mathrm{neck}} = 0.21 \pm 0.01$ Å^{-1}.[17,18]

To understand why the edge of the bulk neck can be seen in the FT-STM images, we return to Eq. (2). Both bulk and surface wave functions have to be matched at the crystal surface with tails decaying into the vacuum. Hence, the STM is able to pick up both bulk and surface-state contributions to the tunnel current at the apex of the tip ($\mathbf{r}_0$), making it possible to see the screening waves created by surface as well as bulk electrons. Following Tersoff and Hamann, we have to evaluate the LDOS at a small distance (r_0) outside the surface in order to calculate the tunnel current. Let the wave functions be of the form

$$\psi = \phi_{\mathbf{q}}(\mathbf{r}_{\parallel}) \exp(-\sqrt{\alpha^2 + q^2}\, z), \tag{3}$$

in which z is the distance above the surface, $\mathbf{q} = \mathbf{k}_{\parallel}$ is the component of the wave vector parallel to the surface, $\phi_{\mathbf{q}}$ is the in-plane part of the wave function, and $\alpha^2 = 2m\phi/\hbar^2$, where ϕ is the work function. We will for simplicity restrict ourselves to the free-electron case.

For a surface state, q has the value dictated by the surface-state dispersion at a given energy E. This yields the surface state ring in the FT-STM image as discussed above. For a bulk state, however, q lies in the range from 0 to $q_E = \sqrt{2mE/\hbar^2}$ since the dispersion is given by $E(k) = \hbar^2(q^2$

$+k_\perp^2)/2m$. Thus, to find the bulk contribution to the LDOS, we have to sum over all qs belonging to the energy E, that is, we have to evaluate

$$\mathrm{LDOS}(E,\mathbf{r}) \propto \int_0^{2\pi} \int_{q_0}^{q_E} |\phi_{\mathbf{q}}|^2 \exp(-2\sqrt{\alpha^2+q^2}z)\, q\ dq\ d\theta. \tag{4}$$

For simplicity, we model the bulk Fermi surface of Au as a sphere with a hole in the top and bottom. Hence, the lower integration limit q_0 corresponds to the radius of the ''neck'' (in the case of a free-electron sphere, we would have $q_0 = 0$). If $\phi_{\mathbf{q}}$ is oscillatory due to the screening of a defect, the resulting LDOS will exhibit oscillations with wave vectors $q = 2k_{\mathrm{neck}}$ and $q = 2k_F$ for $z = 0$. Outside the surface, i.e., for $z > 0$, the exponential term in Eq. (4) kills the contribution from larger wave vectors, and the only oscillation that survives for z larger than ~ 3 Å is the one stemming from the bulk neck. The amplitude fall off is faster than for the pure 2D case because of the bulk (3D) nature of the screening, as discussed in Sec. III. This gives rise to the broader or blurred peak in the FT power spectrum. One should notice that there will be more wave vectors with the magnitude k_{neck} in a model taking into account the actual shape of the bulk Fermi surface because of the neck shape, further enhancing the oscillation with wave vector $q = 2k_{\mathrm{neck}}$. In conclusion, the simple model just described is able to explain the existence of the bulk neck ring in the FT-STM image as well as its broad or blurred appearance. Figure 3(c) schematically illustrates the origin of the two concentric rings in the Au(111) FT-STM image.

The question that remains to be answered is why there is a contribution to the FT-STM image from both the surface Fermi contour and the edge of the bulk Fermi surface neck in some cases, whereas in other cases only the surface contribution is seen.

First, the condition of the tip must play a major role. Unfortunately, it is in general not possible with an STM to control in detail the geometrical and thereby electronic structure of the tip apex. Following the simple model just described, the larger the parallel wave-vector component $k_\parallel$ (q) of the electron is, the smaller is the tunneling probability [see Eqs. (2) and (4)]. This offers some hints to part of an understanding of why in some images only the surface-state contribution is seen. The ''neck electrons'' have larger values of $k_\parallel$, making the contribution to the tunneling current smaller. One could imagine that the (unknown) structure of the tip in some cases impedes the ability to pick up contributions with large $k_\parallel$ components, whereas for other tip conditions electrons with larger values of $k_\parallel$ do contribute. However, we have no detailed control over the tip state, nor do we know the exact interaction of the tip-sample system, and these parameters must be controlled in order to be able to quantitatively understand in detail why the bulk neck contribution to the screening waves is seen only in some cases.

Secondly, defects located slightly below the surface are only screened by bulk electrons since they are not felt by the surface-state electrons. If a large fraction of the defects in the imaged area are located in subsurface sites, the bulk screening contribution may become so large that it compares with the surface-state contribution. It should be noted that the defects still have to be very close to the surface for this explanation to be valid since the imaged bulk screening waves run along the surface layer. This was not the case for the ''vertical'' bulk waves observed in the work of Schmid *et al.*[11] in which Ar bubbles in Al gave rise to screening waves between the bubbles and the surface.

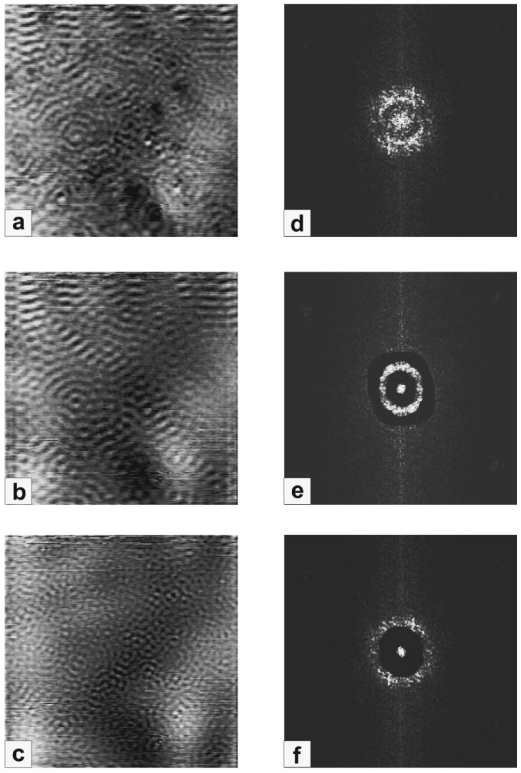

FIG. 5. (a) STM image of Au(111) ($V_t = 0.9$ mV, $I_t = 1.3$ nA, 440×440 Å^2, $T = 150$ K). (b) Surface state contribution to the wave pattern seen in Fig. 5(a). The screening waves from the step just outside the top of the image are very clearly seen. (c) Bulk contribution to the wave pattern seen in Fig. 5(a). Note that practically no waves extend out from the step in the top part of the image. (d)–(f) Fourier transforms of Figs. 5(a)–(c).

The interpretation of the double ring in the case of Cu(111) is exactly the same as the one just presented for the Au(111) case. The Fourier transform depicted in Fig. 4 reveals again two concentric rings. The inner ring is the Fermi contour (scaled with a factor of two) of the surface state centered around $\overline{\Gamma}^8$ ($k_F = 0.21$ Å^{-1}), and contributions from the edge of the bulk neck give rise to the outer ring. The radius of the outer ring is for Cu(111) measured to be $k_{F,\mathrm{outer}} = 0.24 \pm 0.01$ Å^{-1}. This is in good agreement with the value derived from measurements based on the magnetoacoustic effect, $k_{F,\mathrm{neck}} = 0.26 \pm 0.02$ Å^{-1}.[18]

The fact that we observe waves from surface-state electrons as well as bulk electrons allows us to study the role of surface and bulk electrons, respectively, in screening of defects at the surface. With the FT-STM technique, it is possible to identify whether the electrons contributing to the FT-STM image belong to the surface state or the bulk. This is done by means of the lengths of their wave vectors (inner ring: surface state, outer ring: bulk state), and it is then possible to study their behavior independently. By removing the Fourier components belonging to either the surface ring or

the bulk ring and performing an inverse Fourier transform, we obtain a modified direct space image. The resulting changes can be examined, yielding information about which scattering centers are felt by which electrons. As will become clear, we find that bulk electrons do not contribute significantly to the screening of step edges.

To illustrate this, we use the STM image of Au(111) depicted in Fig. 5(a), which shows standing circular waves around defects and a plane wave, in top of the image, originating from a step edge just outside the scanned area. The corresponding FT is shown as Fig. 5(d). To examine the contribution from the surface state, we remove the bulk neck ring and perform the inverse FT. The resulting direct space image and the corresponding FT are shown in Figs. 5(b) and 5(e), respectively. In Fig. 5(b) the plane wave stemming from the step as well as the interference of circular waves around various point scatterers are very clearly seen because of the suppression of the bulk contribution.

If we instead remove the Fourier components representing the surface-state contribution, we obtain the image depicted in Fig. 5(c) with the corresponding FT shown in Fig. 5(f). Most strikingly, the plane-wave train stemming from the step edge has practically disappeared. This means that the potential associated with the step edge does not disturb the bulk state electrons significantly. In general, when comparing the images in Figs. 5(b) and 5(c) (surface and bulk, respectively), it seems that only a few features are screened simultaneously by bulk and surface-state electrons.

Finally, we comment briefly on how the herringbone reconstruction of Au(111) perturbs the screening waves (energy-resolved Friedel oscillations). In Fig. 1(a), the circular wave patterns in the immediate neighborhood of point defects do not seem to be perturbed by or interfere significantly with the reconstruction. In the top left corner of Fig. 1(a), however, the amplitude of the waves is seen to depend on the position relative to the reconstruction lines described in Sec. IV. This effect has previously been addressed by Fujita *et al.*[19] Furthermore, looking in detail at the distribution of Fourier components in Fig. 3(b), there seems to be slightly more intensity in the direction perpendicular to the imaginary line determined by the earlier mentioned reconstruction spots. This means that there are more waves traveling *along* the reconstruction lines than crossing them. This ''wave-guide'' effect of the reconstruction lines has also been discussed by Fujita *et al.*[19] They observed a tendency of the reconstruction lines to steer the standing waves. This effect is not visible in Fig. 3(a) because the image contains several domains of the reconstruction which are ''averaged'' in the Fourier transform.

V. CONCLUSION

In conclusion, we have illustrated the concept of Fourier transforming low bias, constant current STM images showing screening waves, leading to a direct image of the Fermi contour of the surface state. For the first time, we see a bulk contribution to the screening wave pattern, stemming from the edge of the bulk Fermi surface ''neck.'' The measured radius of the neck fits very well in the case of Au(111) and reasonably well in the case of Cu(111). By manipulating the Fourier transform of the images, we can study the bulk and surface contributions to the screening at the surface independently. We find that the bulk electrons do not participate significantly in the screening of the potential associated with step edges.

ACKNOWLEDGMENTS

We gratefully acknowledge stimulating discussions with Phil Sprunger, Phillip Hofmann, and Ward Plummer, as well as financial support from the VELUX Foundation, and the ''Center for Atomic-scale Materials Physics'' (CAMP) sponsored by The Danish National Research Foundation.

[1] J. Lindhard, Dan. Mat. Fys. Medd. **28**, 1 (1954).
[2] N. W. Ashcroft and N. D. Mermin, *Solid State Physics* (Saunders College, Philadelphia, 1976).
[3] G. Grüner, *Density Waves in Solids* (Addison-Wesley, Reading, MA, 1994).
[4] S. D. Kevan, Phys. Scr. **T31**, 32 (1990).
[5] S. D. Kevan, Phys. Rev. Lett. **50**, 526 (1983).
[6] P. T. Sprunger, L. Petersen, E. W. Plummer, E. Lægsgaard, and F. Besenbacher, Science **275**, 1764 (1997).
[7] Ph. Hofmann, B. G. Briner, M. Doering, H.-P. Rust, E. W. Plummer, and A. M. Bradshaw, Phys. Rev. Lett. **79**, 265 (1997).
[8] L. Petersen, P. T. Sprunger, Ph. Hofmann, E. Lægsgaard, B. G. Briner, M. Doering, H.-P. Rust, A. M. Bradshaw, F. Besenbacher, and E. W. Plummer, Phys. Rev. B **57**, R6858 (1998).
[9] M. F. Crommie, C. P. Lutz, and D. M. Eigler, Nature (London) **363**, 524 (1993).
[10] P. Avouris, I.-W. Lyo, R. E. Walkup, and Y. Hasegawa, J. Vac. Sci. Technol. B **12**, 1447 (1994).
[11] M. Schmid, W. Hebenstreit, P. Varga, and S. Crampin, Phys. Rev. Lett. **76**, 2298 (1996).
[12] F. Besenbacher, Rep. Prog. Phys. **59**, 1737 (1996).
[13] J. Friedel, Nuovo Cimento Suppl. **7**, 287 (1958).
[14] J. Tersoff and D. R. Hamann, Phys. Rev. B **31**, 805 (1985).
[15] Y. Hasegawa and Ph. Avouris, Phys. Rev. Lett. **71**, 1071 (1993).
[16] J. V. Barth, H. Brune, G. Ertl, and R. J. Behm, Phys. Rev. B **42**, 9307 (1990).
[17] D. Shoenberg, Philos. Trans. R. Soc. London, Ser. A **255**, 85 (1962).
[18] H. V. Bohm and V. J. Easterling, Phys. Rev. **140**, A2046 (1965).
[19] D. Fujita, K. Amemiya, T. Yakabe, H. Nejoh, T. Sato, and M. Iwatsuki, Phys. Rev. Lett. **78**, 3904 (1997).